Geomechanics and Engineering, *Vol. 19, No. 6 (2019) 485-498*
DOI: https://doi.org/10.12989/gae.2019.19.6.485

Investigating the supporting effect of rock bolts in varying anchoring methods in a tunnel

Hongtao Wang*[1,2], Shucai Li[3], Qi Wang[3], Dechao Wang[4], Weiteng Li[5], Ping Liu[1], Xiaojing Li[1] and Yunjuan Chen[1]

[1]*School of Civil Engineering, Shandong Jianzhu University, Ji'nan 250101, Shandong, China*
[2]*Key Laboratory of Building Structural Retrofitting and Underground Space Engineering (Shandong Jianzhu University), Ministry of Education, Ji'nan 250101, Shandong, China*
[3]*Research Center of Geotechnical and Structural Engineering, Shandong University, Ji'nan 250061, Shandong, China*
[4]*Jinan Rail Transit Group Co., Ltd., Ji'nan 250101, Shandong, China*
[5]*Shandong Provincial Key Laboratory of Civil Engineering Disaster Prevention, Shandong University of Science and Technology, Qingdao 266000, Shandong, China*

(Received March 19, 2018, Revised November 10, 2019, Accepted November 17, 2019)

Abstract. Pre-tensioned rock bolts can be classified into fully anchored, lengthening anchored and point anchored bolts based on the bond length of the resin or cement mortar inside the borehole. Bolts in varying anchoring methods may significantly affect the supporting effect of surrounding rock around a tunnel. However, thus far, the theoretical basis of selecting a proper anchoring method has not been thoroughly investigated. Based on this problem, 16 schemes were designed while incorporating the effects of anchoring length, pretension, bolt length, and spacing, and a systematic numerical experiment was performed in this paper. The distribution characteristics of the stress field in the surrounding rock, which corresponded to various anchoring scenarios, were obtained. Furthermore, an analytical approach for computing the active and passive strengthening index of the anchored surrounding rock is presented. A new fully anchoring method with pretension and matching technology are also provided. Then, an isolated loading model of the anchored surrounding rock was constructed. The physical simulation test for the bearing capacity of the model was performed with three schemes. Finally, the strengthening mechanism of varying anchoring methods was validated. The research findings in this paper may provide theoretical guidelines for the design and construction of bolting support in tunnels.

Keywords: rock bolt; pretension; anchoring method; strengthening index; physical simulation test

1. Introduction

In recent years and with the increase of China's infrastructure construction scale, a large number of highly risky tunnels with very deep depths and complicated geological conditions have emerged in the transportation, water conservancy and hydropower, and mining industries. This creates serious threats for the stability control of surrounding rocks around the tunnel. As an effective supporting technology in tunnel engineering, the use of rock bolts is currently one of the widest applications. By exerting high pretension after installation, rock bolts can provide effective radial constraints for excavated tunnels. Thus, the self-bearing capacity of the surrounding rocks can be enhanced and further deformation and failure of the tunnel can be effectively suppressed.

In mining engineering, resin-anchored rock bolts with small diameter (28–32 mm) boreholes are the preferred type in the roadway support of most coal mines in China (Kang et al, 2013). Such bolts are generally pre-tensioned by tightening the nut. Based on the magnitude of the designed anchoring length of the resin inside the borehole, the bolt is classified into point anchored (the anchoring length is less than or equal to 30% of the borehole length), fully anchored (the anchoring length exceeds 90% of the borehole length) and lengthening anchored bolts (the anchoring length is between the anchoring length of point anchoring and fully anchoring bolts). According to the preceding investigation on some coal mines in Shandong Province of Eastern China (Table 1), we observed that the anchoring length and pretension of the existing rock bolts vary, and the bolt design mainly relies on analogies of experience. Presently, there is no uniform theoretical basis for the proper selection of anchoring methods. For example, the KMG500 high-strength left-hand threaded rebar bolt without a longitudinal bar is employed in the roof support of coal roadways in the Zhaolou coal mine of the Juye mining area. This bolt has a diameter of 22 mm and an anchoring length of 2.1 m. The anchoring length is close to 90% of the rebar. In this anchoring method, the active constraint effect of the bolt pretension may be difficult to exert on the surrounding rocks of the large range, and it may be difficult to enable the bolt and the rock masses to integrate into an effective self-bearing structure. Thus, further discussion is needed to determine whether this anchoring method is reasonable.

The bolting support in tunnel engineering has always been a hotspot of research for many scholars, and various

∗Corresponding author, Ph.D.
E-mail: wanghongtao918@163.com

ISSN: 2005-307X (Print), 2092-6219 (Online)

Table 1 Investigation of the roadway anchoring methods in some coal mines in Shandong Province of Eastern China

Coal mine name	Bolt diameter /mm	Bolt type	Bolt length /m	Anchoring length /m	Pretension /N·m or kN
Zhaolou coal mine	Roof: Φ22	Roof: Left-hand threaded rebar bolt without a longitudinal bar Side: Left-hand fully threaded bolt without a longitudinal bar	2.4	2.1	120 N·m Gob-side entry: 200 N·m
	Side: Φ20		2.0	1.6	60 N·m Gob-side entry: 200 N·m
Jisan coal mine	Roof: Φ22		2.5	2.1	120 N·m
	Side: Φ20		2.2	1.8	60 N·m
Xinglongzhuang coal mine	Φ22		2.5	2.1	100 kN
Longgu coal mine	Φ22	Roof: Left-hand high-strength screw-thread steel Side: Fully threaded bolt with a fine pitch	2.5	1.8	Roof: 400 N·m Side: 300 N·m
Tangkou coal mine	Φ20	Left-hand threaded rebar bolt without a longitudinal bar	2.4	1.0	200 N·m
Liangjia coal mine	Φ18	Round steel twist bolt	2.2	0.7	300 N·m
Guotun coal mine	Φ20	Left-hand threaded rebar bolt without a longitudinal bar	2.4	1.2	260 N·m
Pengzhuang coal mine	Φ20	Fully threaded bolt with iso-strength	2.2	1.2	250 N·m

types of rock bolting technologies have been developed in recent years. For example, Li (2010), Wang *et al.* (2013), He *et al.* (2017), Wang *et al.* (2018), and Li *et al.* (2019) proposed new energy-absorbing bolts or anchor cables to address the large deformation problems of rock masses. Kang *et al.* (2015) developed high-strength rock bolt components and conducted a series of laboratory tests and numerical simulation analyses to study the mechanical behaviors of the new components. Kim *et al.* (2016) proposed an innovative support system that can actively reinforce the weak ground along the whole structural element by introducing an active tension bolt containing a spring unit to the middle of the steel bar to increase its reinforcement capacity. Wang *et al.* (2018, 2019) and Li *et al.* (2020) innovatively applied digital drilling detection test technology to acquire the strength of the broken rock masses and proposed a new high-strength confined concrete support system and bolt-grouting technologies based on traditional bolting support. All of the above-mentioned technologies are of great significance for the effective control of surrounding rocks around the tunnels in complicated geological conditions.

In the theory of rock bolting, Bobet and Einstein (2011), Cai *et al.* (2015), Ranjbarnia *et al.*(2016), Zou *et al.* (2016), Yan *et al.* (2017) and Cui *et al.* (2019) proposed several analytical models for bolted tunnels based on elastic-plastic theory. They obtained the distribution characteristics of rebar axial force and interface shear stress while considering the interaction between bolts and surrounding rock around the tunnel. He *et al.*(2015), Chang *et al.* (2017), Zou and Zhang (2019) and Zhang *et al.* (2020) constructed several new bond-slip models of the bolt-grout interface or the bolt-rock interface, and derived the distribution characteristics of bolt stress under pullout load as well as the curves of axial force and axial displacement by utilizing the load-transfer method. Chen and Li (2015), Ghadimi (2017), Xu *et al.* (2018), Kim *et al.* (2018), Yu *et al.* (2019) and Zuo *et al.* (2019) studied the effect law of these factors, such as varying grouting agents, rebar shape, rebar length, and rebar diameter, on the ultimate bearing capacity of the bolt through laboratory experiments. Nemcik *et al.* (2014) proposed a numerical calculation program of failure propagation for fully grouted rock bolts subjected to a tensile load. Yan *et al.* (2019) proposed a new model for end-anchored rockbolts loaded in tension by implementing a novel tensile failure criterion as part of a 3D continuum numerical modeling package. Kang *et al.* (2016), Liu *et al.* (2017), Wu *et al.* (2018) and Liu *et al.* (2019) investigated the shear behavior of rock bolts. In these research studies, the focus is mainly placed on the stress characteristics or failure mechanisms of the bolt rebar. The mechanical effect of surrounding rock around the tunnel in varying bolting parameters has not been well investigated. Particularly the reasonability of the adopted anchoring methods in Table 1 remains elusive, which is an important reason that the bolting support design is crude and practically empirical. Aiming at this problem, a series of comparison schemes were designed to carry out a systematic numerical experiment in this paper. The effect of the anchoring length, pretension, bolt length, and spacing is incorporated. The distribution characteristics of the supporting stress field in the surrounding rock, which corresponds to varying anchoring scenarios, are investigated. We then propose a theoretical approach for analyzing the strengthening effect of the anchored surrounding rock and obtain an optimal anchoring method. Furthermore, the strengthening effect of varying anchoring methods on the surrounding rock is validated by physical simulation tests. The research findings can serve as a theoretical basis for the design of rock bolting in tunnels or roadways.

2. A numerical experiment for the mechanical effect of varying anchoring methods in a tunnel

2.1 Schematic design and modeling

To investigate the supporting effect of rock bolts in varying anchoring methods in a tunnel, the universal finite difference program FLAC3D is utilized for analysis in this section. A 4 m × 4 m rectangular tunnel was selected as a specific example, and the corresponding numerical calculation model is shown in Fig. 1. Specifically, this model has a size of 40 m × 40 m × 0.8 m (Width × Height × Thickness) and contains 1936 zones. The resin-anchored rock bolts are uniformly arranged along the roof and two sides of the tunnel. By incorporating the effects of anchoring length, pretension, bolt length, and spacing, a total of 16 comparison schemes were designed and are listed in Table 2.

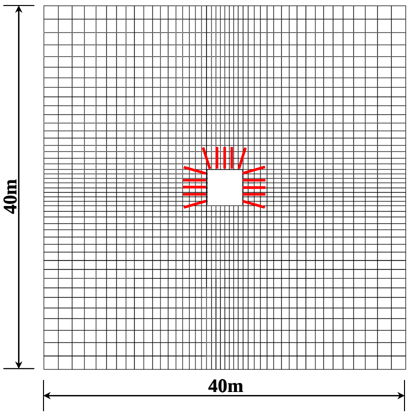

Fig. 1 Numerical calculation model

Table 2 Comparison schemes of the numerical experiment

No.	Anchoring length /m	Pretension /kN	Bolt length /m	Spacing /m
1	0.8	90	2.4	0.8
2	1.2			
3	1.6			
4	2			
5	1.2	30	2.4	0.8
6		60		
7		90		
8		120		
9	0.9	90	1.8	0.8
10	1.2		2.4	
11	1.5		3	
12	1.8		3.6	
13	1.2	90	2.4	0.6
14				0.8
15				1
16				1.2

Table 3 Parameters of the rock bolt

Type	Diameter /mm	Yield strength σ_s /MPa	Ultimate strength σ_b /MPa	Elasticity modulus E /GPa
Resin-anchored rock bolt	ø22	500	700	200

Moreover, to obtain a more universal law, we assume that the surrounding rock around the tunnel is homogeneous and isotropic. The deformation and failure characteristics of the rock masses are simulated through a built-in Mohr-Coulomb constitutive model. The bolts are simulated by using the *CABLE* element. Particularly, the cohesion of the rock mass is 2 MPa, the internal friction angle is 30°, and the tensile strength is 0.4 MPa. The bolt pretension ranges from 30 kN to 120 kN, the anchoring length ranges from 0.8 m to 2.0 m, the bolt length ranges from 1.8 m to 3.6 m, and the bolt spacing ranges from 0.6 m to 1.2 m. The bolt parameters are listed in Table 3.

2.2 Results and analysis

Because the focus in this paper is only placed on the supporting stress field generated by varying anchoring parameters within the surrounding rock, the initial ground stress within the model is neglected in the numerical calculation process. Utilizing the roof surrounding rock within the range of 4 m × 4 m as the research object, Figs. 2-5 depict the compressive stress distribution contours in the surrounding rock under varying schemes. Meanwhile, to facilitate the analysis, we assume that the zone in which the value of the compressive stress is greater than or equal to 0.05 MPa is defined as the effective compression zone. The rock masses within this zone can obtain the effective and active constraint from the bolt pretension, and this is conducive to enabling the rock bolts and surrounding rock to form an effective composite bearing structure.

(1) Effect of the anchoring length

As shown in Fig. 2, the supporting compressive stress generated by the bolt pretension in the surrounding rock mainly focuses on the rock masses at the free part, while the rock masses at the anchored part are mainly subject to tensile stress. The anchoring length has an obvious effect on the distribution of the compressive stress zone. When the anchoring length is 0.8 m, the effective compression zone is approximately 1.7 m in height. When the anchoring length is 2.0 m, the effective compression zone only focuses on the plate and fails to form an effective bearing structure in the anchored surrounding rock. Therefore, from the perspective of enhancing the active supporting effect of rock bolts, the free part with a certain length should be reserved. This is consistent with the theoretical results of Wang *et al.* (2015).

(2) Effect of the pretension

As shown in Fig. 3, when the bolt pretension is relatively small, for example, 30 kN, the effective compression zone in the surrounding rock mainly focuses on the start of the anchored part and the plate. In this case, the effective compression zone is discontinuous and fails to form an effective bearing structure in the anchored surrounding rock. When the bolt pretension is greater than 60 kN, the effective compression zone is continuous, and the magnitude of the compressive stress increases as the pretension increases. For example, when the pretension is 30 kN, the average compressive stress is 0.036 Mpa, whereas the average compressive stress is 0.14 MPa when the pretension is 120 kN.

(3) Effect of the bolt length

It can be seen from Table 2 that the length of the free part increases as the bolt length increases. Accordingly, the effective compression zone in the surrounding rock enlarges with the increase of the bolt length when the pretension is 90kN as shown in Fig. 4. For example, when the bolt length is 1.8 m, the corresponding effective compression zone is only approximately 1 m in height and close to the roof boundary. When the bolt length increases to 3.6 m, the effective compression zone increases to approximately 1.9 m.

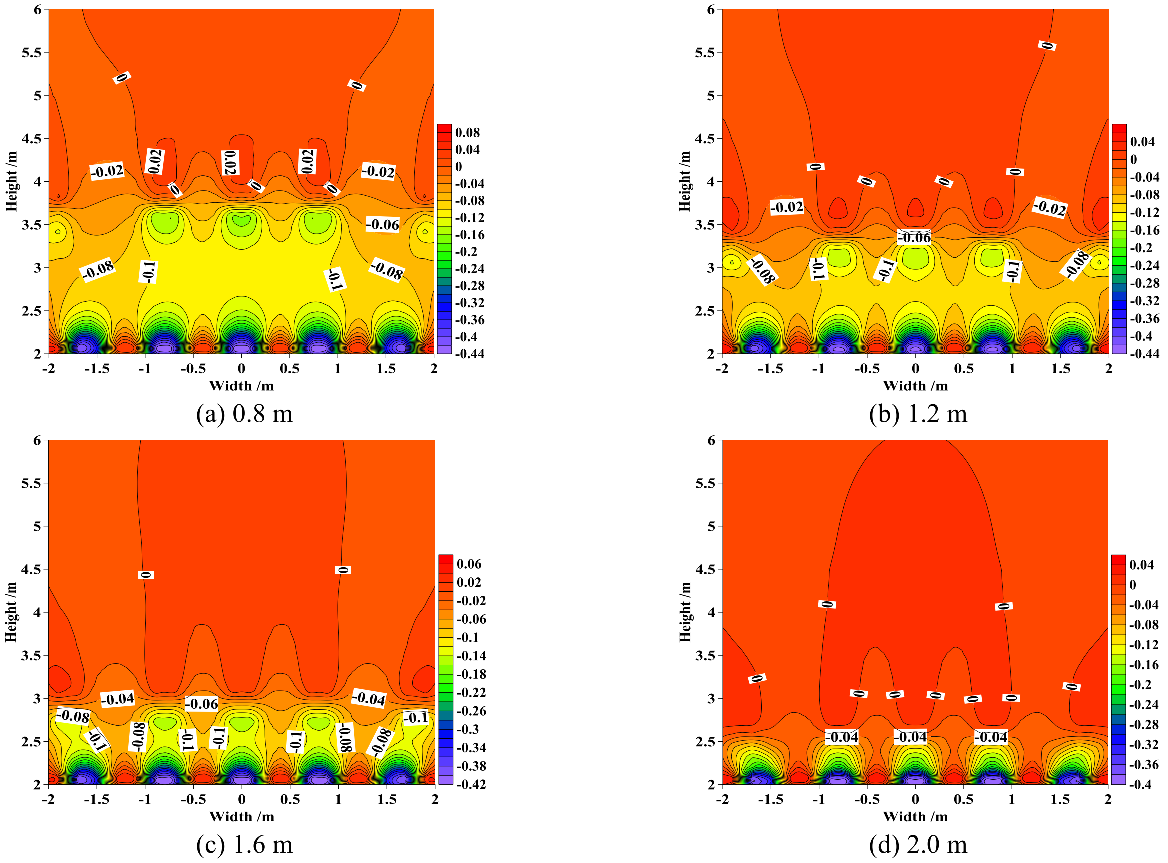

Fig. 2 Stress distribution contours in the surrounding rock under varying anchoring length /MPa

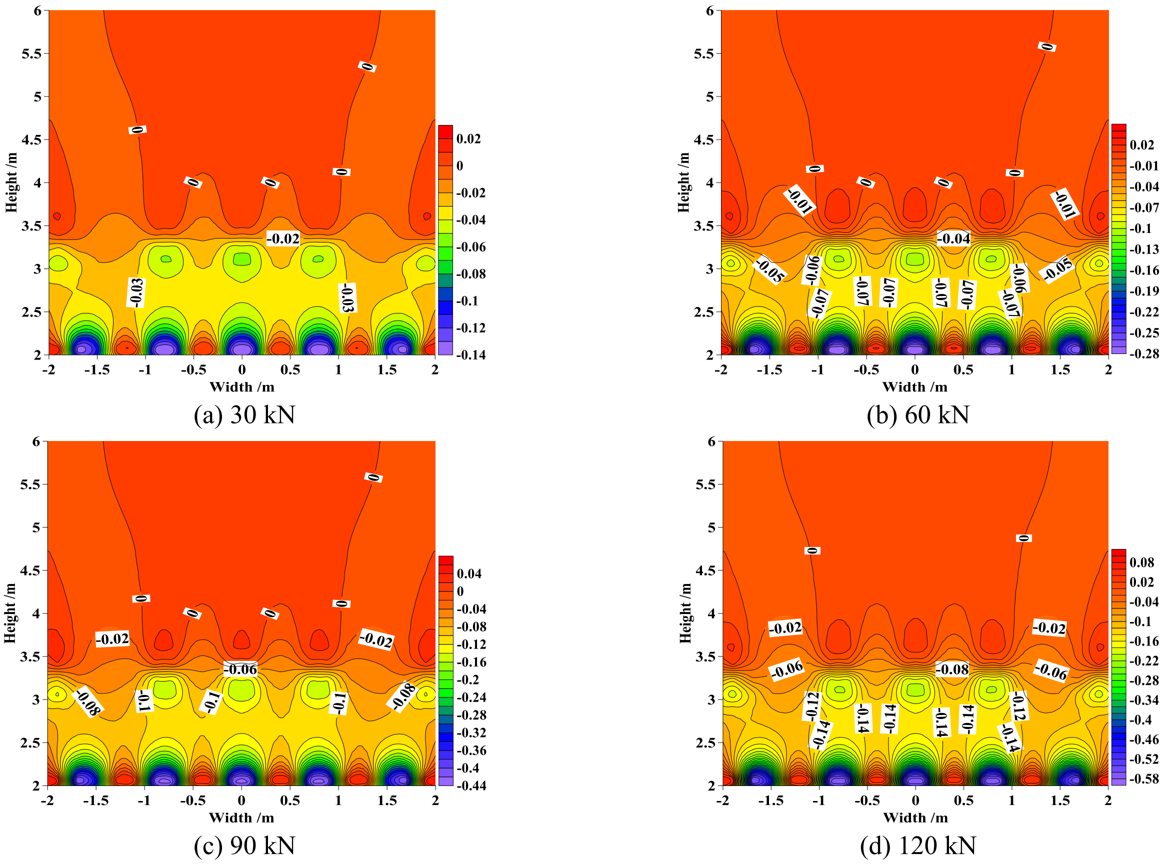

Fig. 3 Stress distribution contours in the surrounding rock under varying pretension /MPa

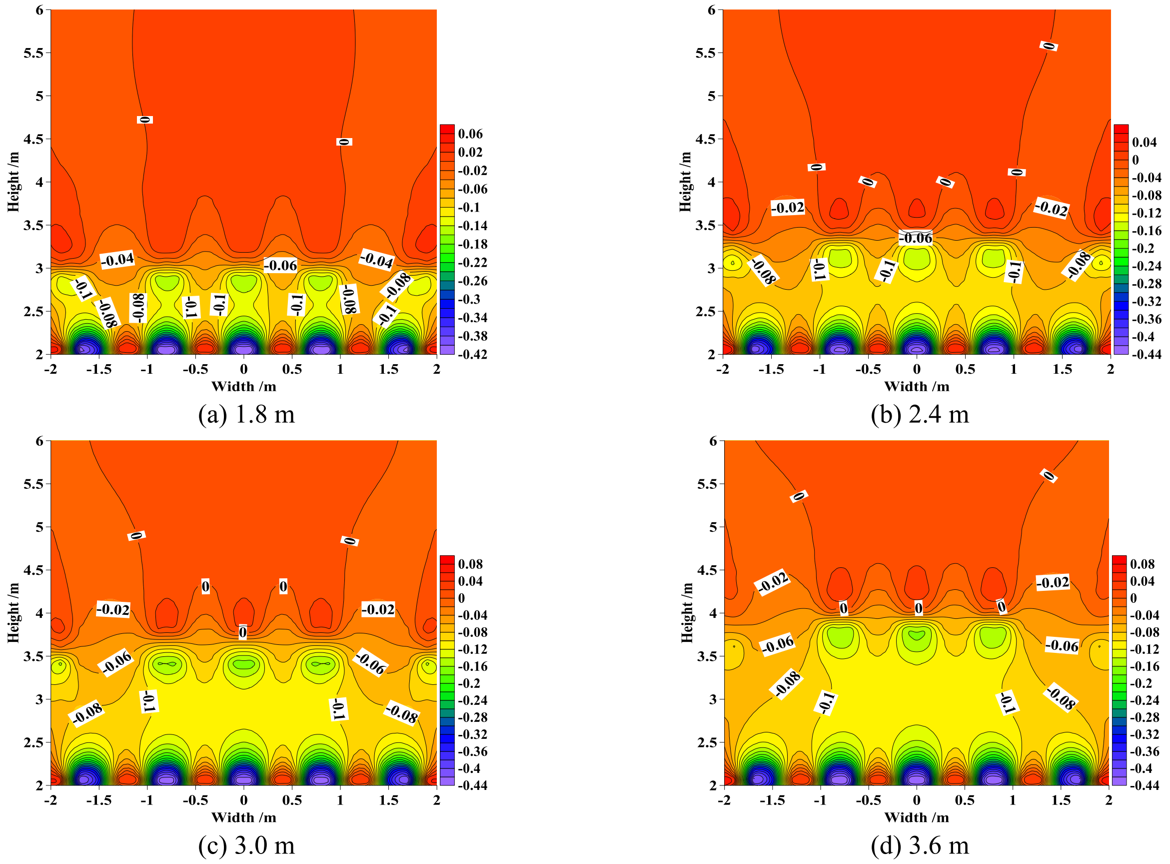

(a) 1.8 m (b) 2.4 m (c) 3.0 m (d) 3.6 m

Fig. 4 Stress distribution contours in the surrounding rock under varying bolt length /MPa

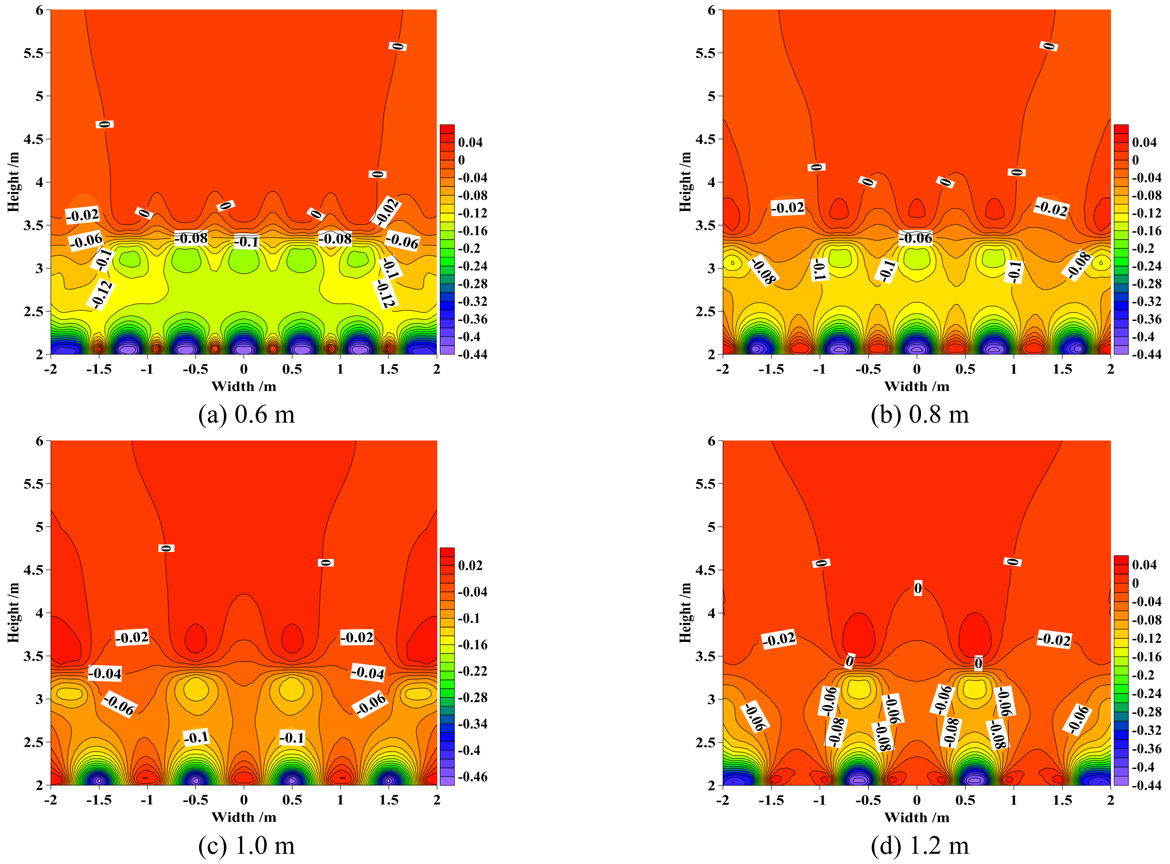

(a) 0.6 m (b) 0.8 m (c) 1.0 m (d) 1.2 m

Fig. 5 Stress distribution contours in the surrounding rock under varying bolt spacing /MPa

(4) Effect of the bolt spacing

As shown in Fig. 5, smaller bolt spacing enables the formation of a continuous compression zone and facilitates the formation of an effective bearing structure in the anchored surrounding rock. For example, when the bolt spacing is less than 1.0 m, the effective compression zone is continuous, whereas the effective compression zone is discontinuous when the spacing is 1.2 m.

3. Theoretical analysis for the strengthening effect of varying anchoring methods

3.1 Supporting effect of the non-fully anchoring method for surrounding rock

According to the preceding results, bolt pretension can only exert an effective constraint on the rock mass at the free part, and the constraint on the rock mass at the anchored part is very limited. Moreover, bolt pretension is exerted before the failure and deformation of the surrounding rock in practical engineering. Specifically, after the tunnel is excavated, a two-dimensional stress state in the surrounding rock close to the tunnel surface may be produced due to the effect of excavation unloading. Then, if the rock bolts are installed and the pretension is applied, an active radial constraint to the tunnel surface can be provided. In this way, the two-dimensional stress state can be converted into the three-dimensional state. In addition, the self-bearing capacity of the surrounding rock can be effectively enhanced. Thus, the supporting effect provided by the pretension along the axial direction in the surrounding rock at the free part can be regarded as an active type.

In addition, it should not be neglected that the anchored part of the bolt also has lateral anti-bending and anti-shearing functions since the surrounding rock and bolt rebar are effectively bonded by the anchoring agent. Specifically, this can prevent the surrounding rock from slipping along the weak plane and further avoid deformation and fracture. However, due to the absence of the anchoring agent at the free part, the anti-bending and anti-shearing functions of the bolt rebar in this zone cannot be effectively exerted. Furthermore, this lateral constraint effect provided by the anchored part is generated after the surrounding rock is deformed. Therefore, such a supporting effect belongs to a passive type.

In summary, the supporting effect provided by the non-fully anchored bolt can be divided into the active effect in the rock mass at the free part and the passive effect in the rock mass at the anchored part. Thus, the passive supporting zone at the anchored part and the active supporting zone at the free part in the surrounding rock around the tunnel in Fig. 1 can be plotted accordingly and as shown in Fig. 6.

3.2 Calculating the strengthening index of the anchored surrounding rock

According to Jing *et al.* (2014), the Mohr-Coulomb strength criterion can be utilized to describe the strengthening effect of rock bolts on surrounding rock. The basic strength parameters of the rock mass include the cohesion and internal friction angle. It can be assumed that the internal friction angle remains constant before and after the bolt is installed, and the strengthening effect can only increase the cohesion of the rock mass. For example, taking the roof surrounding rock within the bolting range in the rectangular tunnel in Fig. 6 as the research object, the contribution of the compressive stress provided by the pretension at the free part and the lateral anti-bending and anti-shearing capacity provided by the rebar at the anchored part to the surrounding rock strength can be calculated as follows.

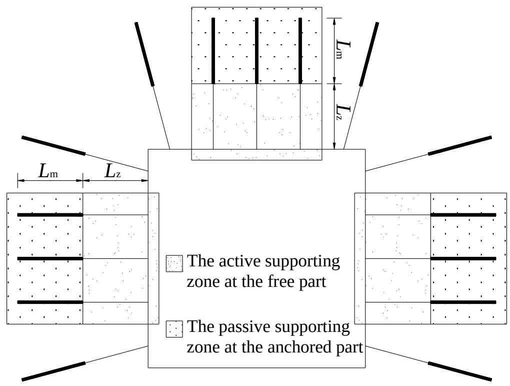

Fig. 6 Division of the supporting zone for the non-fully anchored bolt

(1) Contribution of the compressive stress provided by the axial pretension

The contribution of the bolt pretension on the surrounding rock strength parameters mainly concentrates on the rock mass at the free part. After a tunnel is excavated, the major principal stress in the surrounding rock is parallel to the roof boundary and the minor principal stress is vertical to the roof boundary. Due to the excavation unloading effect, the minor principal stress close to the roof boundary decreases to 0. If the pre-tensioned bolts are installed, then the average supporting compressive stress generated by the pretension is $\bar{p}$ and the range of its influence is L_z in height. Then, according to the Mohr-Coulomb strength criterion, the peak compressive strength σ_{1c} of the rock mass at the free part can be expressed as:

$$\sigma_{1c} = \frac{1+\sin\varphi}{1-\sin\varphi}\bar{p} + \sigma_c \tag{1}$$

where φ refers to the internal friction angle, and σ_c refers to the rock compressive strength without bolting. The magnitude of σ_c can be expressed as:

$$\sigma_c = \frac{2c\cos\varphi}{1-\sin\varphi} \tag{2}$$

where c refers to the cohesion of the rock mass.

Based on Eqs. (1) and (2), the magnitude of the increased compressive strength in the rock mass at the free part can be solved as follows:

$$\Delta\sigma_c = \frac{1+\sin\varphi}{1-\sin\varphi}\bar{p} \tag{3}$$

Table 4 The increased strength parameters of the roof surrounding rock under varying schemes

No.	Bolt quantity	Average compressive stress at the free part $\bar{p}$/MPa	Increased cohesion at the free part Δc_z/MPa	Increased cohesion at the anchored part Δc_m /MPa
1	5	0.106	0.092	0.198
2		0.107	0.093	0.198
3		0.104	0.090	0.198
4		0.112	0.097	0.198
5	5	0.036	0.031	0.198
6		0.071	0.062	0.198
7		0.107	0.093	0.198
8		0.142	0.123	0.198
9	5	0.102	0.089	0.198
10		0.107	0.093	0.198
11		0.105	0.091	0.198
12		0.105	0.091	0.198
13	7	0.140	0.121	0.277
14	5	0.107	0.093	0.198
15	4	0.090	0.078	0.158
16	4	0.073	0.063	0.158

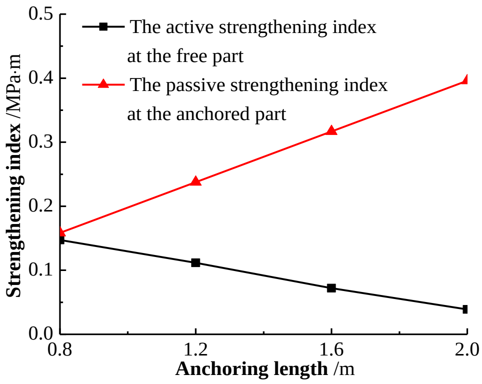

(a) Effect of the anchoring length

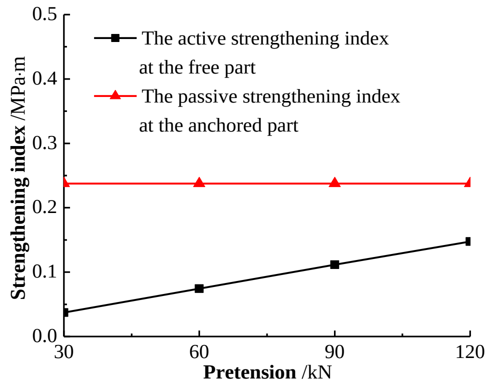

(b) Effect of the pretension

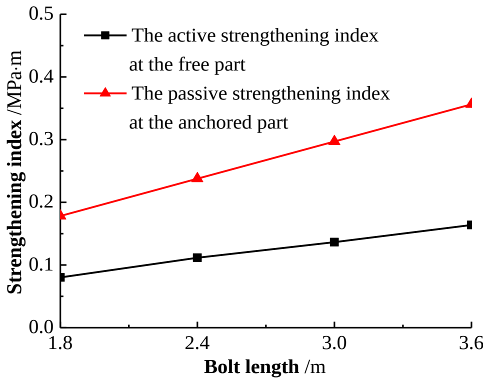

(c) Effect of the bolt length

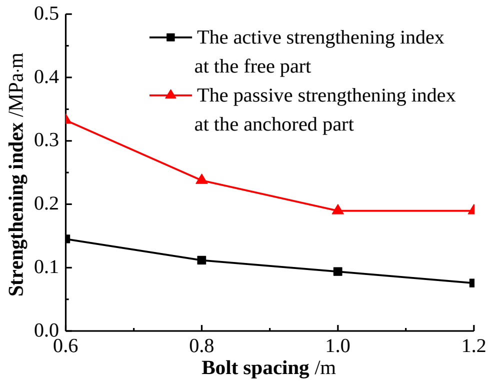

(d) Effect of the bolt spacing

Fig. 7 The strengthening index under varying anchoring parameters

Furthermore, we assume that the composite compressive strength of the anchored surrounding rock can also be expressed as Eq. (2) on the basis of the Mohr-Coulomb strength criterion. Meanwhile, based on the assumption that the internal friction angle of the rock mass remains constant before and after the bolts are installed, the magnitude of the increased compressive strength can also be expressed as:

$$\Delta\sigma_c = \frac{2\Delta c_z \cos\varphi}{1-\sin\varphi} \tag{4}$$

where Δc_z refers to the increased cohesion in the rock mass at the free part. By combining Eqs. (3)and(4), Δc_z results in:

$$\Delta c_z = \frac{1+\sin\varphi}{2\cos\varphi}\bar{p} \tag{5}$$

(2) Contribution of the lateral anti-bending and anti-shearing capacity of the bolt rebar

The contribution of the bolt anti-bending and anti-shearing capacity to the surrounding rock strength parameters mainly concentrates on the rock mass at the anchored part. If the number of the roof bolts is n, the range of its influence at the anchored part is L_m, and the additional cohesion provided by the single bolt is c_m, then the magnitude of the increased cohesion in the rock mass at the anchored part can be expressed as:

$$\Delta c_m = nc_m \tag{6}$$

By referring to the method of Hou and Gou (2000), c_m can be calculated using the following equation:

$$c_m = \frac{\sigma_s \pi b^2}{4\sqrt{3}S\cos(\frac{\pi}{4}-\frac{\varphi}{2})} \tag{7}$$

where σ_s refers to the yield strength of the bolt rebar, b refers to the bolt diameter, and refers to the area of the roof computational region.

(3) The active and passive strengthening index in the surrounding rock

Based on Eqs. (5) and (6), we define the active strengthening index $\Delta\tau_z$ in the rock mass at the free part and the passive strengthening index $\Delta\tau_m$ in the rock mass at the anchored part, respectively, as follows:

$$\begin{cases}\Delta\tau_m = L_m \Delta c_m \\ \Delta\tau_z = L_z \Delta c_z\end{cases} \tag{8}$$

where the strengthening index indicates the magnitude of the increased strength parameters in the anchored surrounding rock and the range of the effective supporting zone.

3.3 Effect of varying anchoring parameters on the strengthening index

Based on the numerical simulation results in section 2, the average compressive stress $\bar{p}$ in the roof surrounding rock at the free part under varying schemes can be obtained. Then, the increased strength parameters in the anchored surrounding rock can be solved by using Eqs. (5) and (6) as listed in Table 4.

Furthermore, by using Eq. (8), we can calculate the magnitude of the active and passive strengthening index corresponding to varying schemes. The variation curves of the strengthening index are shown in Fig. 7.

We observe from Table 4 and Fig. 7 that both the free part and the anchored part of the rock bolts are conducive to an increase of the rock strength parameters (to a certain extent). Specifically, with the increase of the anchoring length, the active strengthening index at the free part decreases, and the passive strengthening index at the anchored part increases, whereas the increase of the pretension can only enhance the active strengthening index and the passive strengthening index is not affected. Furthermore, with an increase of the bolt length and a decrease of the bolt spacing, the active and passive strengthening index are effectively enhanced.

4. Presenting the new fully anchoring method

According to the preceding analysis and for the non-fully anchored bolt, decreasing the anchoring length was shown to effectively increase the active strengthening index in the surrounding rock. However, the passive strengthening index could be reduced as the anchoring length decreases. This seems to be contradictory. To solve this problem, we propose a new anchoring method in this paper. Particularly, we assume that the optimal anchoring method should enable the support potential of the bolt rebar at the free part and the anchored part to be completely exerted. Namely, the active strengthening index at the free part and the passive strengthening index at the anchored part should simultaneously reach a maximum value. Furthermore, this can be accomplished through the new fully anchoring method with pretension (the point anchored bolt with filling of the free part) as shown in Fig. 8.

Fig. 8 shows that the new fully anchoring method consists of inner and outer anchored parts. Practically, the following two construction methods can be employed to obtain the supporting effect of the new fully anchoring method.

One method is to employ two types of resin capsules with varying solidification speeds as shown in Fig. 9. After the borehole is drilled, the fast and slow solidification resin capsules are put into the borehole in sequence. Then, the bolt is installed using a jumbolter. In this process, the resin capsules are mashed. The fast and slow solidification filling sections are formed from inside to outside along the borehole. In addition, the pretension is exerted on the bolt after the inner filling section is solidified and before the

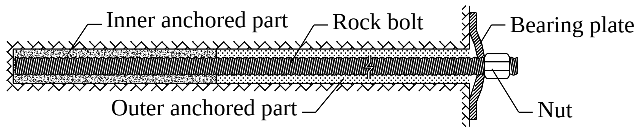

Fig. 8 The new fully anchoring method

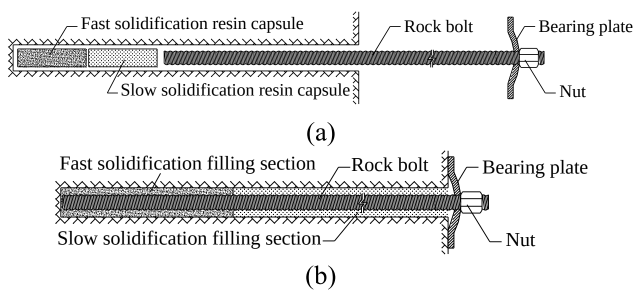

Fig. 9 The new fully anchoring method achieved by fast and slow solidification resin capsules

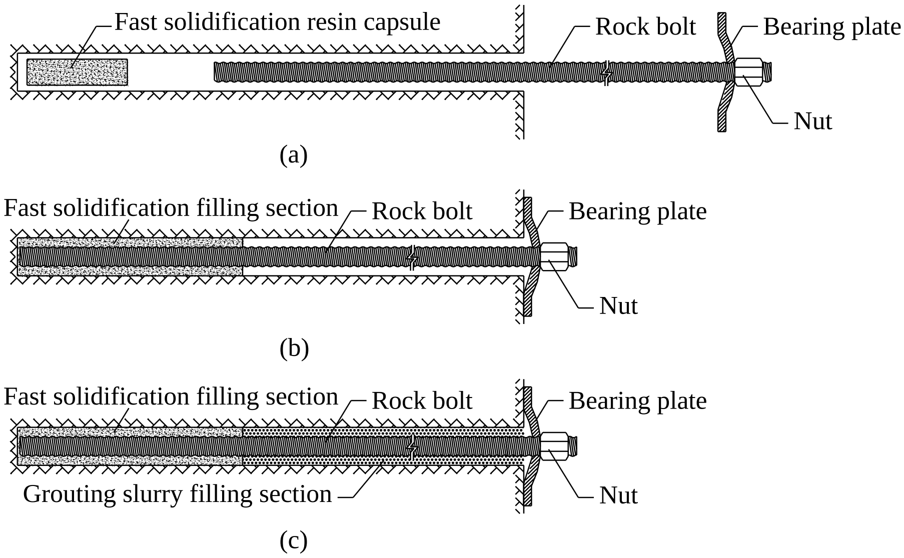

Fig. 10 The new fully anchoring method achieved by the fast solidification resin capsule and grouting

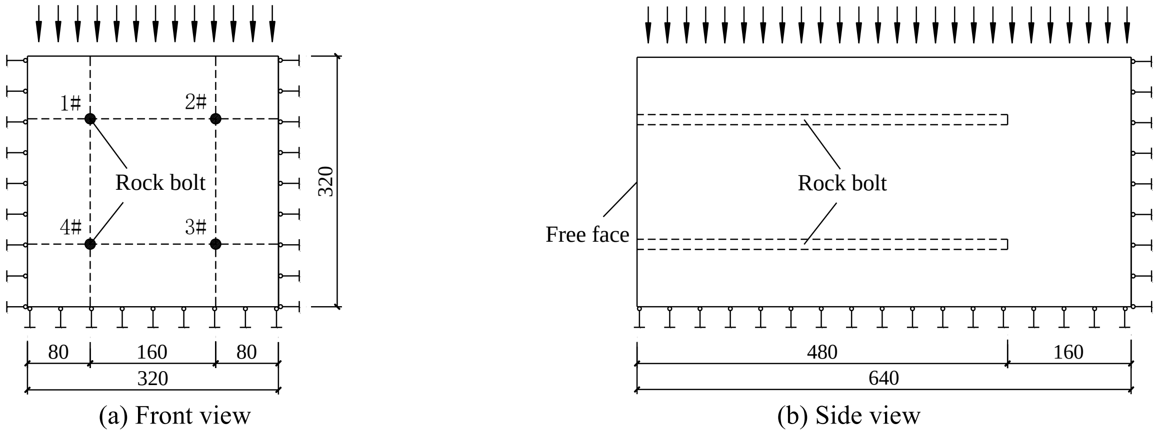

Fig. 11 The size and loading scheme of the isolated model

outer filling section is solidified. The supporting effect of the fully anchoring method can be achieved after the outer filling section is solidified.

Another method is to employ the fast solidification resin capsule combined with grouting as shown in Fig. 10. After the inner filling section with the fast solidification resin capsule is solidified and the pretension is exerted to the bolt, the surrounding rock can be grouted through the borehole at the free part. The grouting slurry can fill both the borehole at the free part and the cracks in the surrounding rock. Then, the integrity and strength of the surrounding rock can be effectively enhanced.

Compared with the conventional non-fully anchored bolt, the pretension in the new fully anchoring method is exerted after the inner anchored part is solidified and before the outer anchored part is formed. Setting a small inner anchored part, such as point anchoring, can enable the pretension to adequately diffuse into the surrounding rock and effectively enhance the active strengthening index. Meanwhile, after the outer anchored part is solidified, the bolt installation is completed. The total anchoring length is equal to the borehole length. In this case, the lateral anti-bending and anti-shearing capacity along the full length of the rebar can be completely exerted, and the corresponding passive strengthening index in the surrounding rock is maximized. In addition, this type of anchoring method can also effectively avoid rebar corrosion and the loss of pretension.

Specifically, in tunnel support design, the length of the inner anchored part can be set to a value between 1/4 and 1/3 of the bolt length (as for the soft rock, the larger value should be chosen), the pretension can be set to 60-120 kN, and the recommended bolt spacing should not exceed 1.0 m. Meanwhile, the bolt pretension must be designed with a comprehensive consideration of factors such as the rebar strength and tenacity. To achieve a supporting effect of high pretension, a bolt with high strength and high tenacity is preferred. In addition, the broken degree of the rock masses in tunnels is also a key factor for determining whether an effective bearing structure can be formed in the anchored surrounding rock. When the surrounding rock shows good integrity, the first fully anchoring method mentioned above can be utilized. When the surrounding rock is broken, the fully anchoring method based on grouting can be utilized and thus increase the integrity and self-bearing capacity of the surrounding rock.

5. Verification by the physical simulation test

5.1 Loading model and schematic design

To further verify the strengthening mechanism of the surrounding rock in varying anchoring methods, a physical simulation test was conducted in this section. Specifically, we separated a certain range of rock masses from the roof or two sides of the tunnel in Fig. 1 and scale it down to construct an isolated model as shown in Fig. 11. The size of this model is 320 mm × 320 mm × 640 mm (Width × Height × Length). The uniformly arranged bolts in the model have a length of 480 mm with a spacing of 160 mm. The outer surface close to the outer end of the bolt is the tunnel free face. The bottom surface, two side surfaces and rear surface of the model are fixed with no displacement. Three schemes are designed in total as shown in Table 5. After the bolts are installed, a destructive test was conducted by loading pressure from the top surface to investigate the deformation characteristics and bearing capacity of the surrounding anchored rock.

The physical model is made through layered filling and compaction with a mixture of cement, gypsum, and river sand. Specifically, the model material ratio is as follows: the ratio of sand to binder is 6:1, the ratio of cement to gypsum is 6:4, and the ratio of water to material is 0.07. Accordingly, the model unit weight ranges from 16.8 $kN \cdot m^{-3}$ to 17.2 $kN \cdot m^{-3}$, the elasticity modulus ranges from 142 MPa to 178 MPa, the compressive strength ranges from 0.88 MPa to 0.95 MPa, the tensile strength ranges from 0.05 MPa to 0.08 MPa, the cohesion ranges from 0.19 MPa to 0.25 MPa, and the frictional angle ranges from 31°to 34°.

The bolt is simulated by adopting the φ6 mm threaded rod and the matching bearing plate and nut. The bolt is installed by utilizing a high-strength resin and pretensioned by tightening the nut. Specifically and to simulate the non-fully anchored bolt in scheme 2, lubricating oil is evenly applied to the bolt surface at the free part. As for the anchored part, resin with grit is applied to the bolt surface the first time. When the bolt is installed, resin is applied to the bolt surface for the second time. In scheme 3, lubricating oil is not applied to the bolt surface at the free part. After the bolt is installed and pretension is exerted, cement grout is injected into the borehole at the free part to simulate the new fully anchored bolt.

5.2 Testing system and monitoring components

To achieve the loading and testing of the physical models, the simulation testing system for the anchored surrounding rock was developed as shown in Fig. 12. The testing system consists of a counter-force loading device, a mobile mould, a servo oil-pressure control system, and a multi-element real-time monitoring system with high accuracy.

With a size of 1500 mm × 1500 mm × 1000 mm (Width × Height × Thickness), the main frame of the counter-force loading device is composed of beams, stand columns, and reinforcing plates with ribbed bottoms. Meanwhile, to achieve a true simulation of the boundary conditions of stress loading and reduce the boundary effect, a flexible uniform pressure loading device developed by Li *et al.* (2015) is employed in the testing system as shown in Fig. 13. Particularly, this device includes three oil cylinders in the horizontal direction and three oil cylinders in the vertical direction. Moreover, each oil cylinder is equipped

Table 5 Physical simulation test schemes in varying anchoring methods

No.	Schematic Design
1	The model without bolting.
2	The model with an anchoring length of 0.24 m and a pretension of 0.70 kN.
3	The model with an anchoring length of 0.24 m and a pretension of 0.70 kN. The free part is filled with cement grout.

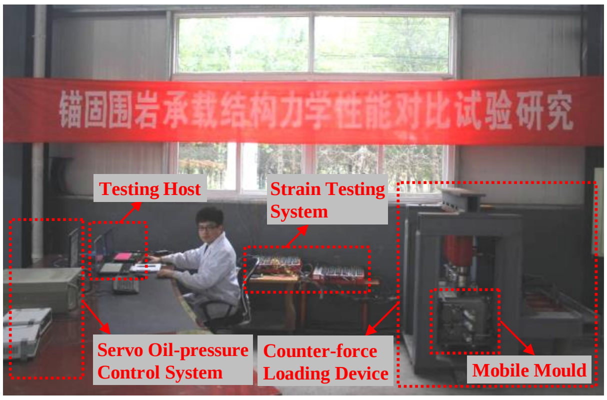

Fig. 12 Simulation testing system

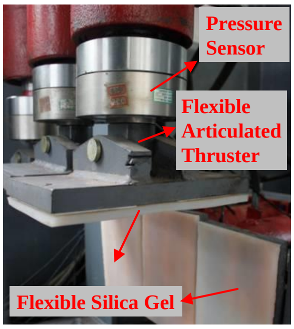

Fig. 13 Flexible uniform pressure loading device

Fig. 14 Loading and testing of the isolated model

(a) The model without bolting

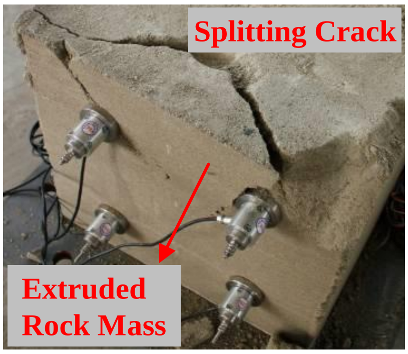

(b) The model with bolting

Fig. 15 Typical failure patterns of the isolated models

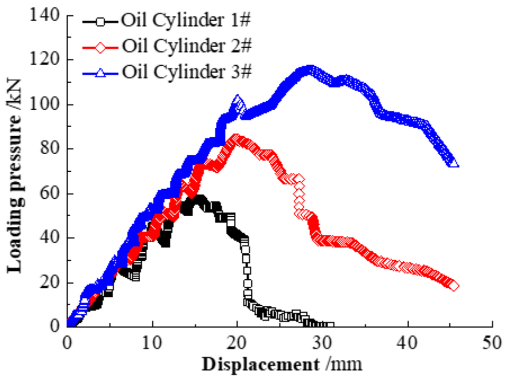

(a) Scheme 1

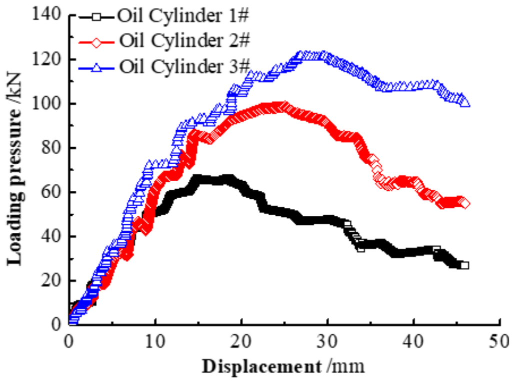

(b) Scheme 2

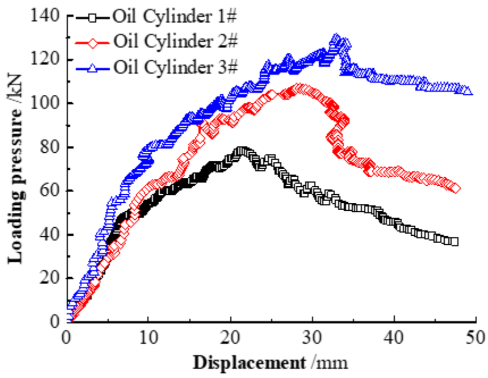

(c) Scheme 3

Fig. 16 Monitoring curves of the top loading pressure under varying schemes

Table 6 Peak and residual loading pressures of the models in scheme 1-3

No.	Oil cylinder 1#		Oil cylinder 2#	
	Peak pressure /kN	Residual pressure /kN	Peak pressure /kN	Residual pressure /kN
1	56.9	6.2	84.5	25.6
2	67.3	33.2	98.7	58.8
3	77.1	39.7	106.8	64.4

with a flexible articulated thruster with a size of 300 mm × 200 mm (Length × Width) and silica gel with the thickness of 15 mm. By cooperating with the servo oil-pressure control system, the whole testing system can achieve functions of asynchronous loading and pressure that are maintained at the horizontal and vertical directions.

During the test, the physical model is constructed in the mobile mould in advance. Then, it is moved into the internal space of the counter-force loading device for loading and testing. In the loading process, the top loading pressure, deformation at the free face, and the bolt force are simultaneously monitored. Fig. 14 shows the loading and testing of the physical model.

5.3 Test results and analysis

Fig. 15 shows the typical failure patterns of the models without bolting in scheme 1 and with bolting in scheme 2. Fig. 16 shows the monitoring curves of the loading pressure of the top three oil cylinders versus the extruded displacement at the free face in scheme 1, 2, and 3, wherein the serial number of the top oil cylinders from outside to inside is 1# - 3# in sequence.

We observed that the physical models in scheme 1, 2 and 3 present obvious splitting failure characteristics under top loading pressure. When the loading pressure is relatively small, the rock mass close to the model free face is the first to split. With the increase of the loading pressure, the splitting scope gradually extends towards the interior, and the rock mass at the free face is extruded. In this process and after the emergence of splitting, the model without bolting collapse showed obvious brittle failure. Then, the bearing capacity rapidly decreases. However, the model with bolting does not collapse due to the constraint effect of the bolts. Instead, the bolt can adjust and improve the stress state of the interior rock mass. The model can form an effective bearing structure interiorly with the bolt and rock mass, which enables the model to present ductility deformation behavior and post-peak bearing capacity. This effectively restricts further breakage inside the model.

Furthermore, using the rock mass within the scope of bolting as the research object, Table 6 lists the peak and residual loading pressure of oil cylinder 1# to 2# in scheme 1, 2, and 3.

Table 6 shows that the pre-tensioned bolts can effectively increase the peak and post-peak bearing capacity of the models. For example, the peak and residual pressures of oil cylinder 1# in scheme 2 are higher than those in scheme 1 by 18.3% and 435.5%, respectively. The peak and residual pressures of oil cylinder 1# in scheme 3 are higher than those in scheme 1 by 35.5% and 540.3%, respectively. Furthermore, the free part of the bolts in scheme 3 is filled with cement grout after the pretension is exerted. In this way and upon the precondition of ensuring the effective diffusion of the pretension, the bolts can effectively enable the lateral anti-bending and anti-shearing functions along the whole length and further increase the integral rigidity of the model. Accordingly, both the peak and residual pressure of the model in scheme 3 is greater than that in scheme 1 and scheme 2. This also validates the effectiveness of the preceding theoretical analysis results and the superiority of the new fully anchoring method.

6. Conclusions

Through a systematic numerical experiment, this paper investigated the distribution characteristics of the supporting stress field in surrounding rock around a tunnel and corresponding to varying anchoring length, pretension, bolt length, and spacing. Then, an analytical approach for computing the strengthening index of the anchored surrounding rock and a new fully anchoring method are presented. Furthermore, we perform a physical simulation test for the bearing capacity of the anchored surrounding rock to validate the effectiveness of the theoretical analysis results. The major conclusions are as follows:

- For the non-fully anchored bolt, the active constraining effect of the pretension on the surrounding rock is mainly within the scope of the rock mass at the free part, while the active constraining effect on the rock mass at the anchored part is very limited. This is conducive to the diffusion of pretension and forming an effective bearing structure in the surrounding anchored rock by employing high pretension and reserving a certain length of the free part.
- The strengthening effect of the non-fully anchored bolt for the surrounding rock is classified into the passive strengthening effect at the anchored part and the active strengthening effect at the free part. With an increase of the anchoring length, the active strengthening index decreases and the passive strengthening index increases. In addition, increasing the pretension can only enhance the active strengthening index. The overall strengthening index is enhanced with an increase of the bolt length and a decrease of the bolt spacing.
- The optimal anchoring method should enable the support potential of the bolt rebar at the free part and the anchored part to be completely exerted. Accordingly, a new fully anchoring method with pretension (the point anchored bolt filling the free part) can be employed to achieve an optimal supporting effect.
- The pre-tensioned bolt may enable the surrounding rock to present certain characteristics of ductility deformation. Both the peak and residual bearing capacity of the anchored surrounding rock can be effectively enhanced and compared with unanchored surrounding rock.
- Since the free part of the bolt is filled with cement grout in the new fully anchoring method, the integral rigidity of the surrounding rock is enhanced. Accordingly, the peak and residual bearing capacity of the surrounding rock are greater than those using the non-fully anchoring method.

Acknowledgments

The authors express sincere appreciation to the reviewers for their valuable comments and suggestions that helped to improve the quality of the paper. The authors also would like to acknowledge the financial support from the National Natural Science Foundation of China (Nos. 51704177, 51809159, 51604166, 51609130), a Project of Shandong Province Higher Educational Science and Technology Program (J16LG04), Shandong Co-Innovation Center for Disaster Prevention and Mitigation of Civil Structures (XTP201911), and the Doctoral Research Fund of Shandong Jianzhu University (XNBS1501).

References

Bobet, A. and Einstein, H.H. (2011), “Tunnel reinforcement with rockbolts”, *Tunn. Undergr. Sp. Technol.*, **26**(1), 100-123. https://doi.org/10.1016/j.tust.2010.06.006.

Cai, Y., Jiang, Y., Djamaluddin, I., Iura, T. and Esaki, T. (2015), "An analytical model considering interaction behavior of grouted rock bolts for convergence–confinement method in tunneling design", *Int. J. Rock Mech. Min. Sci.*, **76**, 112-126. https://doi.org/10.1016/j.ijrmms.2015.03.006.

Chang, X., Wang, G., Liang, Z., Yang, J. and Tang, C. (2017), "Study on grout cracking and interface debonding of rockbolt grouted system", *Constr. Build. Mater.*, **135**, 665-673. https://doi.org/10.1016/j.conbuildmat.2017.01.031.

Chen, Y. and Li, C.C. (2015), "Performance of fully encapsulated rebar bolts and D-Bolts under combined pull-and-shear loading", *Tunn. Undergr. Sp. Technol.*, **45**, 99-106. https://doi.org/10.1016/j.tust.2014.09.008.

Cui, L., Zheng, J.J., Sheng, Q. and Pan, Y. (2019), "A simplified procedure for the interaction between fully-grouted bolts and rock mass for circular tunnels", *Comput. Geotech.*, **106**, 177-192. https://doi.org/10.1016/j.compgeo.2018.10.008.

Ghadimi, M. (2017), "Effect of profile bolt in bond strength fully grouted rock bolts using analytical and experimental methods", *Int. J. Min. Miner. Eng.*, **8**(2), 156-168.

He, L., An, X.M. and Zhao, Z.Y. (2015), "Fully grouted rock bolts: an analytical investigation", *Rock Mech. Rock Eng.*, **48**(3), 1181-1196. https://doi.org/10.1007/s00603-014-0610-0.

He, M., Li, C., Gong, W.L., Sousa, L.R. and Li, S.L. (2017), "Dynamic tests for a constant-resistance-large-deformation bolt using a modified SHTB system", *Tunn. Undergr. Sp. Technol.*, **64**, 103-116. https://doi.org/10.1016/j.tust.2016.12.007.

Hou, C.J. and Gou, P.F. (2000), "Mechanism study on strength enhancement for the rocks surrounding roadway supported by bolt", *Chin. J. Rock Mech. Eng.*, **19**(3), 342-345.

Jing, H.W., Yang, S.Q., Zhang, M.L., Xu, G.A. and Chen, K.F. (2014), "An experimental study on anchorage strength and deformation behavior of large-scale jointed rock mass", *Tunn. Undergr. Sp. Technol.*, **43**, 184-197. https://doi.org/10.1016/j.tust.2014.05.006.

Kang, H., Wu, Y., Gao, F., Jiang, P., Cheng, P., Meng, X. and Li, Z. (2016), "Mechanical performances and stress states of rock bolts under varying loading conditions", *Tunn. Undergr. Sp. Technol.*, **52**, 138-146. https://doi.org/10.1016/j.tust.2015.12.005.

Kang, H., Wu, Y., Gao, F., Lin, J. and Jiang, P. (2013), "Fracture characteristics in rock bolts in underground coal mine roadways", *Int. J. Rock Mech. Min. Sci.*, **62**, 105-112. http://dx.doi.org/10.1016%2Fj.ijrmms.2013.04.006.

Kang, H., Yang, J. and Meng, X. (2015), "Tests and analysis of mechanical behaviours of rock bolt components for China's coal mine roadways", *J. Rock Mech. Geotech. Eng.*, **7**(1), 14-26. https://doi.org/10.1016/j.jrmge.2014.12.002.

Kim, H.J., Kim, K.H., Kim, H.M. and Shin, J.H. (2018), "Anchorage mechanism and pullout resistance of rock bolt in water-bearing rocks", *Geomech. Eng.*, **15**(3), 841-849. https://doi.org/10.12989/gae.2018.15.3.841.

Kim, S.H., Song, K.I. and Park, J.H. (2016), "Experimental evaluation of the active tension bolt", *Geomech. Eng.*, **11**(2), 177-195. https://doi.org/10.12989/gae.2016.11.2.177.

Li, C.C. (2010), "A new energy-absorbing bolt for rock support in high stress rock masses", *Int. J. Rock Mech. Min. Sci.*, **47**(3), 396-404. https://doi.org/10.1016/j.ijrmms.2010.01.005.

Li, S.C., Wang, Q., Wang, H.T., Jiang, B., Wang, D.C., Zhang, B., Li, Y. and Ruan, G.Q. (2015), "Model test study on surrounding rock deformation and failure mechanisms of deep roadways with thick top coal", *Tunn. Undergr. Sp. Technol.*, **47**, 52-63. https://doi.org/10.1016/j.tust.2014.12.013.

Li, W., Yang, N., Mei, Y., Zhang, Y., Wang, L. and Ma, H. (2020), "Experimental investigation of the compression-bending property of the casing joints in a concrete filled steel tubular supporting arch for tunnel engineering", *Tunn. Undergr. Sp. Technol.*, **96**, 103184. https://doi.org/10.1016/j.tust.2019.103184.

Li, Z.H., Lv, Q., Zhu H.X. and Hu J. (2019), "Laboratory testing and modeling of a high-displacement cable bolt", *Int. J. Geomech.*, **19**(7), 04019078. https://doi.org/10.1061/(ASCE)GM.1943-5622.0001472.

Liu, J., Yang, H., Wen, H. and Zhou, X. (2017), "Analytical model for the load transmission law of rock bolt subjected to open and sliding joint displacements", *Int. J. Rock Mech. Min. Sci.*, **100**, 1-9. https://doi.org/10.1016/j.ijrmms.2017.01.018.

Liu, S., Fu, M., Jia, H. and Li, W. (2019), "Shear Characteristics of Cuneiform Reaming Anchorage Bolts in Coal Mine Roadways", *Rock Mech. Rock Eng.*, **52**(6), 1931-1943. https://doi.org/10.1007/s00603-018-1670-3.

Nemcik, J., Ma, S., Aziz, N., Ren, T. and Geng, X. (2014), "Numerical modelling of failure propagation in fully grouted rock bolts subjected to tensile load", *Int. J. Rock Mech. Min. Sci.*, **71**, 293-300. https://doi.org/10.1016/j.ijrmms.2014.07.007.

Ranjbarnia, M., Oreste, P., Fahimifar, A. and Arya, A. (2016), "Analytical-numerical solution for stress distribution around tunnel reinforced by radial fully grouted rockbolts", *Int. J. Numer. Anal. Meth. Geomech.*, **40**(13), 1844-1862. https://doi.org/10.1002/nag.2517.

Wang, G., Wu, X.Z., Jiang, Y.J., Huang, N. and Wang, S.G. (2013), "Quasi-static laboratory testing of a new rock bolt for energy-absorbing applications", *Tunn. Undergr. Sp. Technol.*, **338**, 122-128. https://doi.org/10.1016/j.tust.2013.05.010.

Wang, H.T., Wang, Q., Wang, F.Q., Li, S.C., Wang, D.C., Ren, Y.X., Guo, N.B. and Zhang, S.G. (2015), "Mechanical effect analysis of bolts in roadway under different anchoring lengths and its application", *J. China Coal. Soc.*, **40**(3), 509-515.

Wang, Q., Gao, H.K., Yu, H.C., Jiang, B. and Liu, B.H. (2019), "Method for measuring rock mass characteristics and evaluating the grouting-reinforced effect based on digital drilling", *Rock Mech. Rock Eng.*, **52**, 841-851. https://doi.org/10.1007/s00603-018-1624-9.

Wang, Q., He, M.C., Yang, J., Gao, H.K., Jiang, B. and Yu H.C. (2018), "Study of a no-pillar mining technique with automatically formed gob-side entry retaining for longwall mining in coal mines", *Int. J. Rock Mech. Min. Sci.*, **110**, 1-8. https://doi.org/10.1016/j.ijrmms.2018.07.005.

Wang, Q., Jiang, B., Pan, R., Li, S.C., He, M.C., Sun, H.B., Qin, Q., Yu, H.C. and Luan, Y.C. (2018), "Failure mechanism of surrounding rock with high stress and confined concrete support system", *Int. J. Rock Mech. Min. Sci.*, **102**, 89-100. https://doi.org/10.1016/j.ijrmms.2018.01.020.

Wang, Q., Qin, Q., Jiang, B., Yu, H.C., Pan, R. and Li, S.C. (2019), "Study and engineering application on the bolt-grouting reinforcement effect in underground engineering with fractured surrounding rock", *Tunn. Undergr. Sp. Technol.*, **84**, 237-247. https://doi.org/10.1016/j.tust.2018.11.028.

Wu, X., Jiang, Y. and Li, B. (2018), "Influence of joint roughness on the shear behaviour of fully encapsulated rock bolt", *Rock Mech. Rock Eng.*, **51**(3), 953-959. https://doi.org/10.1007/s00603-017-1365-1.

Xu, C., Li, Z., Wang, S., Wang, S., Fu, L. and Tang, C. (2018), "Pullout performances of grouted rockbolt systems with bond defects", *Rock Mech. Rock Eng.*, **51**(3), 861-871. https://doi.org/10.1007/s00603-017-1373-1.

Yan, Q., Li, S.C., Xie, C. and Li, Y. (2017), "Analytical solution for bolted tunnels in expansive loess using the convergence-confinement method", *Int. J. Geomech.*, **18**(1), 04017124. https://doi.org/10.1061/(ASCE)GM.1943-5622.0000989.

Yan, S., Song, Y., Bai, J. and Elmo, D. (2019), "A study on the failure of resin end-anchored rockbolts Subjected to tensile load", *Rock Mech. Rock Eng.*, **52**(6), 1917-1930. https://doi.org/10.1007/s00603-018-1663-2.

Yu, S., Zhu, W., Niu, L., Zhou, S. and Kang, P. (2019), "Experimental and numerical analysis of fully grouted long rockbolt load-transfer behavior", *Tunn. Undergr. Sp. Technol.*, **85**, 56-66. https://doi.org/10.1016/j.tust.2018.12.001.

Zhang, W., Huang, L. and Juang, C.H. (2020), "An analytical model for estimating the force and displacement of fully grouted rock bolts", *Comput. Geotech.*, **117**, 103222. https://doi.org/10.1016/j.compgeo.2019.103222.

Zou, J.F. and Zhang, P.H. (2019), "Analytical model of fully grouted bolts in pull-out tests and in situ rock masses", *Int. J. Rock Mech. Min. Sci.*, **113**, 278-294. https://doi.org/10.1016/j.ijrmms.2018.11.015.

Zou, J.F., Xia, Z.Q. and Dan, H.C. (2016), "Theoretical solutions for displacement and stress of a circular opening reinforced by grouted rock bolt", *Geomech. Eng.*, **11**(3), 439-455. https://doi.org/10.12989/gae.2016.11.3.439.

Zuo, J.P., Wen, J.H., Li, Y.D., Sun, Y.J., Wang, J.T., Jiang, Y.Q. and Liu, L. (2019), "Investigation on the interaction mechanism and failure behavior between bolt and rock-like mass", *Tunn. Undergr. Sp. Technol.*, **93**, 103070. https://doi.org/10.1016/j.tust.2019.103070.

CC